Hindawi Publishing Corporation
Mathematical Problems in Engineering
Volume 2015, Article ID 251906, 12 pages
http://dx.doi.org/10.1155/2015/251906

Research Article

Dynamic Modeling and Control Strategy Optimization for a Hybrid Electric Tracked Vehicle

Hong Wang,[1] Qiang Song,[1] Shengbo Wang,[2] and Pu Zeng[3]

[1]*Beijing Co-Innovation Center of Electric Vehicles, National Engineering Laboratory for Electric Vehicles, Beijing Institute of Technology, No. 5 South Zhongguancun Street, Haidian District, Beijing 100081, China*
[2]*Construction Machinery R&D Center, Intelligence Research Department, Shantui Construction Machinery Co., Ltd., No. 58 Highway G327, Jining, Shandong 272073, China*
[3]*Shanghai Volkswagen, Ningbo 315336, China*

Correspondence should be addressed to Qiang Song; songqiang@bit.edu.cn

Received 5 June 2015; Revised 20 September 2015; Accepted 21 September 2015

Academic Editor: Xiaosong Hu

A new hybrid electric tracked bulldozer composed of an engine generator, two driving motors, and an ultracapacitor is put forward, which can provide high efficiencies and less fuel consumption comparing with traditional ones. This paper first presents the terramechanics of this hybrid electric tracked bulldozer. The driving dynamics for this tracked bulldozer is then analyzed. After that, based on analyzing the working characteristics of the engine, generator, and driving motors, the power train system model and control strategy optimization is established by using MATLAB/Simulink and OPTIMUS software. Simulation is performed under a representative working condition, and the results demonstrate that fuel economy of the HETV can be significantly improved.

1. Introduction

As a type of construction vehicle, the quantity of bulldozers is increasing significantly with tremendous social development, usually causing energy unsustainability and poor air quality. Additionally, the energy efficiency of the conventional bulldozer is only 20%. The electrification of the bulldozer as construction machinery is a good way to decrease air pollution and oil shortages. For these reasons, developing an electric bulldozer has significant effects on energy savings and emission reductions [1]. Studies have been performed to address these energy issues, notably regarding the utilization of electricity as a viable replacement of oil. Hybrid power systems are more suitable than traditional power trains for the reduction of fuel consumption and emissions. In the United States, Caterpillar produced the first D7E hybrid electric drive tracked bulldozer in March 2008. Compared with traditional models, CO and NO_x emissions were reduced by approximately 10% and 20%, respectively. The D7E can improve fuel economy by 25% [2].

Hybrid electric tracked bulldozer is a complex system due to its two power sources: engine-generator sets and ultracapacitor. The working speeds of the engine and charge-discharge properties of the ultracapacitor impact the fuel economy of the bulldozer together. A reasonable energy distribution control strategy could achieve the minimum fuel consumption. How to coordinate the power flow between engine-generator sets, ultracapacitor, and drive motor effectively to achieve the minimum fuel consumption is a complex design optimization problem.

In recent years, scholars have proposed a variety of different power allocation control strategies for electric vehicles [3–8], which can be roughly classified into two categories: thermostat type and power follow type [9–12]. The working principle of the thermostat type control strategy is as follows: engine outputs a set constant power when the SOC of battery is lower than the set minimum value; engine does not work when SOC is higher than the set maximum value. At this time, the battery needs to meet the transient high power discharge requirements that could do harm to the discharge

efficiency and the lifetime of the battery. Power follow control strategy requires the engine-generator sets output power to always follow the load demand power of the vehicle, causing engine speed frequently fluctuate and affecting the engine efficiency and emission properties. Xiong et al. [13] adopted the thermostat control strategy for PHEV, taking battery and ultracapacitor as the auxiliary power source. This control method improved the discharge efficiency and the lifetime of the auxiliary power source. However, it is complex, rarely used in the construction machinery vehicles, like bulldozer. Kwon et al. [14] adopted power follow control strategy for a series hybrid wheel excavator, taking ultracapacitor as the auxiliary power source which improved the fuel economy by 24%. However, this control method limited the improvement of the fuel economy as engine was controlled to work at one single point.

In this paper, one power follow control strategy is put forward to combine the working features of the proposed series hybrid electric tracked bulldozers [15, 16]. Bulldozers do not require high speed and acceleration performance. But they demand power when low-speed operation fluctuates remarkably. Considering working features of the bulldozer, ultracapacitor is taken as the auxiliary power source due to its high power density and short-term high power and current output capabilities. By analyzing the engine-generator working point and the SOC state of the ultracapacitor, a reasonable power control strategy is proposed to improve the fuel economy of the hybrid electric tracked bulldozer. Test bench experiment was performed to collect actual test bench data to correlate and validate the proposed control strategy for this hybrid electric tracked bulldozer.

Parameter optimization for the power follow control strategy is also researched because of the importance of accurate match of control strategy parameters for fuel economy improving [17, 18]. Commonly, genetic algorithm is famous for its global optimization and parallel computing capabilities [19–21] and has been widely used in multiple areas, including parameter estimation in system identification, optimization, and neural network training [22]. A genetic algorithm is established to solve the parameter optimization problem in the control strategy in this study.

The organization of this paper is as follows. In Section 2, the new configuration of the hybrid electric tracked bulldozer is described and the detailed terramechanics of the tracked bulldozer is researched to provide the theoretical basis for the modeling of the dynamics in Section 3. The power control strategy is described in Section 4. The optimization problem, procedure, and results of the control strategy are introduced in Section 5. Finally, the conclusions are presented in Section 6.

2. Terramechanics of the Tracked Bulldozer

2.1. Configuration of the Hybrid Electric Tracked Bulldozer. The schematic of this hybrid electric tracked bulldozer (using one traditional bulldozer as the prototype) is given in Figure 1. This hybrid electric tracked bulldozer maintains the vehicle body, hydraulic and operation system of the traditional bulldozer, just changing the transmission form. The paths for the electric power and mechanical power are tandem in the series configurations. This construction simplifies the propulsion and transmission system and provides greater flexibility in the power train system.

This hybrid electric tracked bulldozer uses an integrated controller to control two motors on both sides of the bulldozer independently and to transfer electric energy from the DC BUS into mechanical energy to drive the bulldozer.

The terramechanics of this hybrid electric tracked bulldozer is the theoretical basis for further analysis of the driving dynamics. The working states of the tracked bulldozer can be divided into the following six stages: soil-cutting, soil-transportation, returning, climbing, turning, and accelerating. The external travel resistance, operating resistance, driving force, and track slide curve under the working states are researched in the following context.

2.2. External Travel Resistance, F_E. The resistance caused by the vertical deformation of the soil under the anterior track of the vehicle when driving is called external travel resistance. It mainly results from the energy consumption of soil compaction and the effects of bulldozing resistance. F_E can be written as the following [23]:

$$\begin{aligned} F_E &= F_c + F_b, \\ F_c &= \frac{2b}{(n+1)\,k^{1/n}} \left(\frac{G}{2bL}\right)^{(n+1)/n}, \\ F_b &= \gamma Z^2 b k_\gamma + 2bZck_{\mathrm{pc}}, \end{aligned} \tag{1}$$

where

$$\begin{aligned} k_\gamma &= \left(\frac{2N_\gamma}{\tan\psi} + 1\right)\cos^2\psi, \\ k_{\mathrm{pc}} &= (N_c - \tan\psi)\cos^2\psi, \end{aligned} \tag{2}$$

where F_c is compaction resistance (N); F_b is bulldozing resistance (N); b is track width (m); G is vehicle weight (N); L is track length (m); c is soil cohesion coefficient (KPa); ψ is soil internal friction angle (°); n is soil deformation index; k is soil deformation modulus (KN/m^{n+2}); Z is track amount of sinkage (m); γ is unit weight (N/m^3); and N_γ and N_c are the soil Terzaghi coefficients of bearing capacity [24].

2.3. Operating Resistance F_T. Consider

$$\begin{aligned} F_T &= F_1 + F_2 + F_3 + F_4, \\ F_1 &= 10^6 B_1 h_p k_b, \\ F_2 &= G_t \mu_1 \cos\alpha = \frac{V\gamma\mu_1\cos\theta}{k_s}, \\ F_3 &= 10^6 B_1 X \mu_2 k_y, \\ F_4 &= G_t \mu_2 \cos\delta^2 \cos\theta, \\ V &= \frac{B_1\left(H - h_p\right)^2 k_m}{2\tan\alpha_0}, \end{aligned} \tag{3}$$

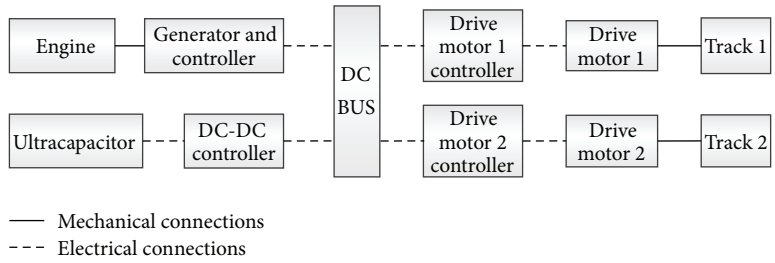

Figure 1: Configuration of hybrid electric tracked bulldozer.

where F_1 is soil-cutting resistance (N); F_2 is the pushing resistance of the mound before the blade (N); F_3 is frictional resistance between the ground and blade (N); F_4 is the horizontal component of the frictional resistance when the soil rises along the blade (N); k_b is cutting resistance per unit area (MPa); B_1 is blade width (m); h_p is average cutting depth (m); G_t is the gravity of the mound in front of the bulldozing plate; μ_1 is the friction coefficient between soil particles; μ_2 is the friction coefficient between the soil and blade; θ is slope (°); V is the volume of the mound in front of the bulldozing plate; k_s is the loose degree coefficient of the soil; k_m is the fullness degree coefficient of the soil; H is blade height (m); α_0 is the natural slope angle of the soil (°); k_y is cutting resistance per unit area after the blade is pressed into the soil (MPa); X is the length of the worn blade contacting the ground (m); and δ is the cutting angle of the blade (°) [1].

2.4. Driving Force, F. The soil driving force is partly consumed by overcoming external travel resistance and bulldozer operation, acceleration, climbing, or load traction. The relationship between maximum driving force (adhesion force) $F_{\max}$ and slide ratio i is given as the following [25]:

$$F_{\max} = 2bLc\left(1 + \frac{2h}{b}\right) + G\tan\varphi\left\{1 + 0.64\left[\frac{h}{b}\operatorname{arc\,cot}\left(\frac{h}{b}\right)\right]\right\}. \quad (4)$$

Thus, driving force F can be written as the following:

$$F = F_{\max}\left[1 - \frac{K}{iL}\left(1 - e^{-iL/K}\right)\right], \quad (5)$$

where h is the grouser height (m) and K is the soil horizontal shear deformation modulus (m):

$$i = 1 - \frac{v}{r_0\omega_0} = 1 - \frac{v}{v_T} = \frac{v_T - v}{v_T} = \frac{v_j}{v_T}, \quad (6)$$

where v is the actual speed of vehicle (m/s); ω_0 is the angular velocity of the sprocket wheel (rad/s); r_0 is the pitch radius of the sprocket wheel (m); v_T is the theoretical speed of vehicle; v_j is the track slip velocity relative to the ground (rad/s).

2.5. Track Slide Curve. Based on the parameters of the bulldozer and sandy loam shown in Table 1, the track slide curve of this hybrid electric tracked bulldozer on sandy loam is shown in Figure 2.

Table 1: Parameters of the bulldozer and soil.

Name	Value	Unit
Vehicle weight (G)	280	KN
Track width (b)	0.61	m
Track length (L)	3.05	m
Grouser height (h)	0.07	m
Soil cohesion coefficient (c)	13.79	KPa
Soil internal friction angle (ψ)	28	Degree
Soil deformation index (n)	0.3	Null
Soil deformation modulus (k)	146	KN/m^{n+2}
Unit weight (γ)	17700	N/m^3
Soil Terzaghi coefficients of bearing capacity (N_c)	10.8	Null
Soil Terzaghi coefficients of bearing capacity (N_r)	3.8	Null
Soil horizontal shear deformation modulus (K)	0.02	m

From Figure 2, the driving force reaches a maximum of 213 KN when the track slips completely (slide ratio $i = 1$, meaning that the track slip velocity relative to the ground is equal to the theoretical speed of vehicle), and the difference between the driving force and external travel resistance is used for the operation, acceleration, climbing, and load traction of the bulldozer.

3. Dynamic Modeling of the Hybrid Electric Tracked Bulldozer

The series hybrid power system is composed of a diesel engine, permanent magnet generator, motor drive system, and tracks, as shown in Figure 1. The hybrid electric bulldozer uses the integrated controller to control the motors on both sides of the bulldozer independently and to transfer the electric energy from the generator and auxiliary power supply (also from DC BUS) into mechanical energy to drive the bulldozer [26]. Based on the working principle analysis and test bench experiment of various parts of the power train system, a mathematical model of the hybrid power system was established.

3.1. Engine-Generator Model. To ensure the accuracy of the modeling, test bench experimental data are used to establish

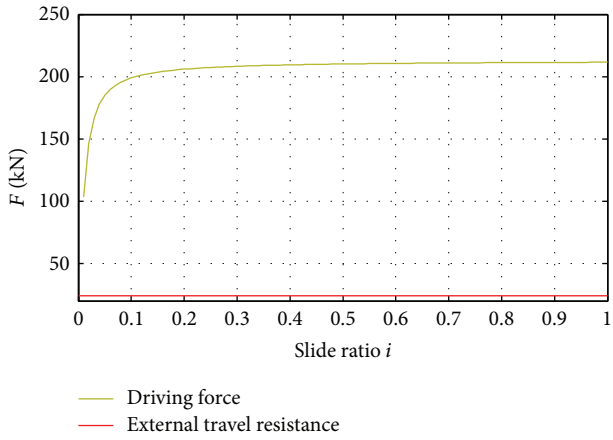

Figure 2: Track slide curve of the tracked bulldozer on sandy loam.

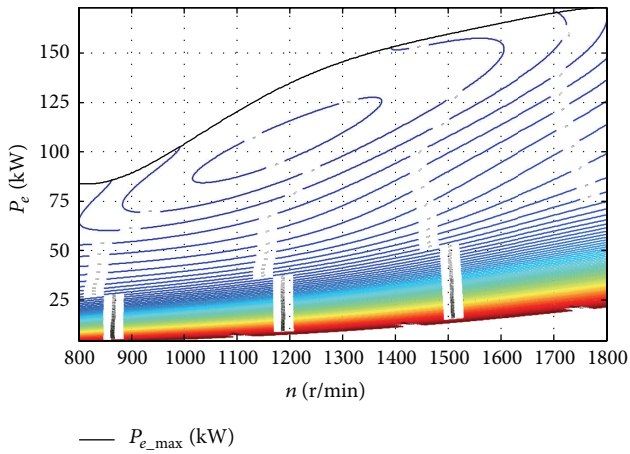

Figure 3: Diesel engine universal characteristic curve.

the diesel engine universal characteristic curve, as shown in Figure 3.

The engine fuel injection amount is determined by throttle position and engine speed. Engine output torque is determined by the following:

$$T_e^D = T_e - J_e \frac{dw_e}{dt},$$
$$T_e = \alpha * T_{e\_\max}(n_e), \tag{7}$$

where T_e^D is dynamic engine output torque; T_e is steady-state engine flywheel output torque; α is throttle position; $T_{e\_\max}(n_e)$ is maximum torque at the engine speed n_e; and J_e is the rotary inertia of the rotating parts in the engine.

The engine fuel consumption b_e (g/kWh) is a function of T_e and n_e:

$$b_e = f(T_e, n_e) = \sum_{j=0}^{s} \sum_{i=0}^{j} A_k * T_e^i * n_e^{j-1} \tag{8}$$
$$(i, j = 0, 1, 2, \ldots, s),$$

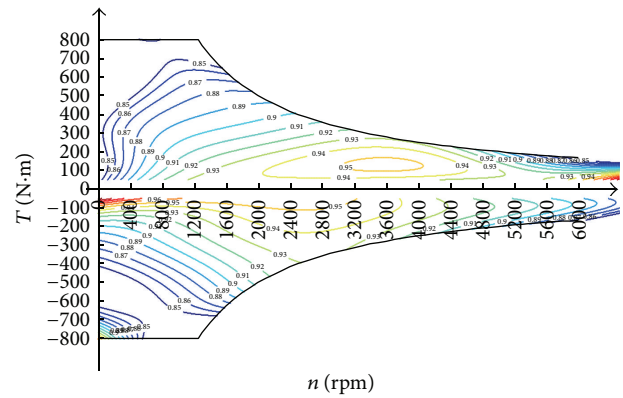

Figure 4: Motor drive system efficiency.

where s is model order number and A_k is the polynomial coefficient $k = (j^2 + j + 2 * i)/2$.

The generator provides current to DC BUS under generating mode; the kinetic equation for the generator is given as the following:

$$J_g \frac{dn_g}{dt} = T_g - T_e^D, \tag{9}$$

where T_g is generator shaft torque; n_g is generator speed; and J_g is the rotary inertia of the generator.

The relationship between generator shaft torque, speed and output DC voltage, and current of the controller side is given as the following:

$$\frac{U_g \cdot I_g}{1000 \cdot \eta_g} = \frac{T_g \cdot n_g}{9549}, \tag{10}$$

where U_g is output DC voltage from the generator; I_g is output DC current; η_g is power generation efficiency.

3.2. Motor Model. A permanent magnet motor is adopted in this hybrid bulldozer with a torque of 500/800 N·m, a power of 75/105 kW, a rated speed of 1430 rpm, and a maximum speed of 6000 rpm. In this power train system, the two motors follow the instructions of the control unit for torque output. The focus of the motor model is to establish the relationship between the output torque, speed of the motor and the input DC voltage, and current of the motor controller. Therefore, the motor model is obtained based on the test bench data of the motor drive system. Figure 4 shows the efficiency map of the system.

Considering the response time of the motor drive system, a first-order link is added between the target torque and the actual output torque:

$$T_m = \begin{cases} \dfrac{T_{\text{ref}}}{\tau s + 1} & T_{\text{ref}} \le T_{\max}(n) \\ \dfrac{T_{\max}(n)}{\tau s + 1} & T_{\text{ref}} > T_{\max}(n), \end{cases} \tag{11}$$

where T_{ref} is target torque; T_m is output torque; n is motor speed; $T_{\max}(n)$ is maximum torque at speed n; and τ is response time.

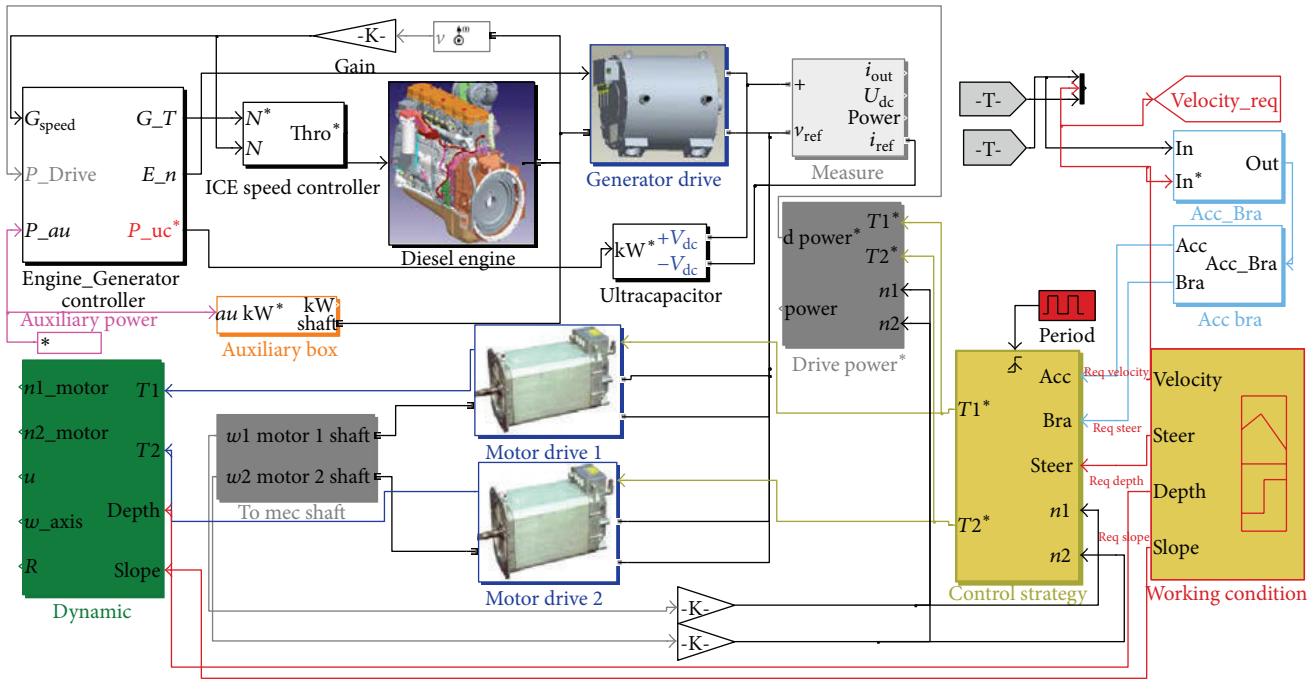

FIGURE 5: The power train system model of the hybrid electric tracked bulldozer.

The dynamic equation for the motor is as follows:

$$J_m \frac{dn}{dt} \frac{2\pi}{60} = T_m - T_{\text{load}}, \tag{12}$$

where J_m is motor rotational inertia and T_{load} is load torque.

The relationship between the input DC voltage, current of the motor controller and the shaft output torque, and speed is as follows:

$$\begin{aligned} \frac{U \cdot I \cdot \eta_d}{1000} &= \frac{T_m \cdot n}{9549} \quad (T_m > 0), \\ \frac{U \cdot I}{1000 \cdot \eta_b} &= \frac{T_m \cdot n}{9549} \quad (T_m < 0), \end{aligned} \tag{13}$$

where U is the input DC voltage; I is the input DC current; η_d is motor efficiency when driving; and η_b is motor efficiency when braking.

3.3. Driving Dynamic Model. Based on the study of the terramechanics of this hybrid electric tracked bulldozer, a driving dynamic model is established as follows:

$$\begin{aligned} (T_1 + T_2) \frac{i_0 \eta}{r} - R_L - R_R &= m\dot{v}, \\ (T_1 - T_2) \frac{i_0 \eta}{r} \frac{B}{2} + (R_L - R_R) \frac{B}{2} - T_r &= I\dot{w}, \\ T_r &= \begin{cases} 0, & w = 0, \\ \dfrac{\mu l m g}{4} \left[1 - \left(\dfrac{2\lambda_1}{l} \right)^2 \right], & w \neq 0, \end{cases} \end{aligned} \tag{14}$$

where $T_{1,2}$ is motor output torque; i_0 is the gear ratio from the motor to the driving wheel; η is the efficiency from the motor shaft to the track; r is driving wheel radius; R_L and R_R are left and right side track resistance, respectively; m is vehicle mass; v is the vehicle drive speed along the longitudinal direction; T_r is steering resistance torque; I is vehicle rotational inertia; w is vehicle angular velocity; μ is steering resistance coefficient; l is vehicle length; and λ_1 is the offset of the track contact with the ground alone longitudinal direction.

The power train system simulation model of the hybrid electric tracked bulldozer including the driver model, working condition model, engine-generator model, motor drive system model, vehicle dynamics model, and control strategy in MATLAB/Simulink is shown in Figure 5, where (1)~(3) and (14) are used in the module "dynamic"; (7)~(8) are used in the module "diesel engine"; (9)~(10) are used in the module "generator drive"; (11)~(13) are used in the module "motor drive 1" and "motor drive 2."

3.4. Experiment Validity Analysis of the Dynamic Model of the Hybrid Bulldozer. To verify the accuracy of the simulation model of the hybrid electric tracked bulldozer, the parameters and the real working conditions (as shown in Figure 6) were substituted into this simulation model to compare the simulation results with the real vehicle experimental data.

In Figure 6, V (km/h) is the bulldozer velocity; depth (m) is soil-cut depth; and slope (°) is bulldozer gradeability. The working stages are described as follows: 1~4 s traveling stage; 4~16 s soil-cutting stage; 16~31 s soil-transportation stage; 31~33 s unloading soil stage; and 33~50 s no-load stage.

Figures 7 and 8 show the simulation result and real bulldozer's working velocities and drive forces of single track

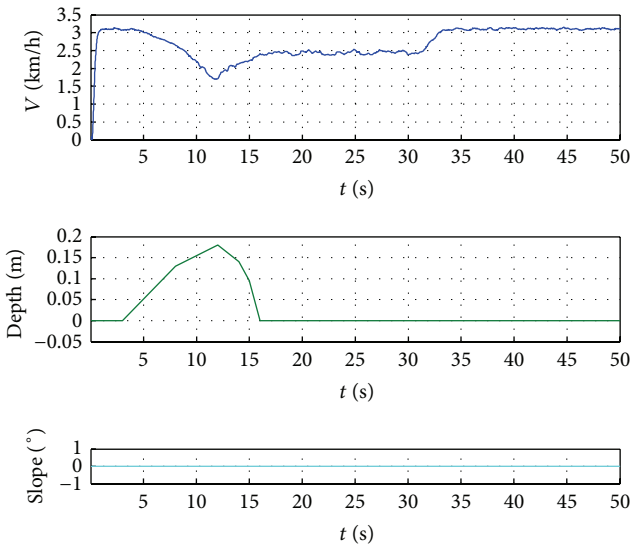

Figure 6: The real working condition of the bulldozer.

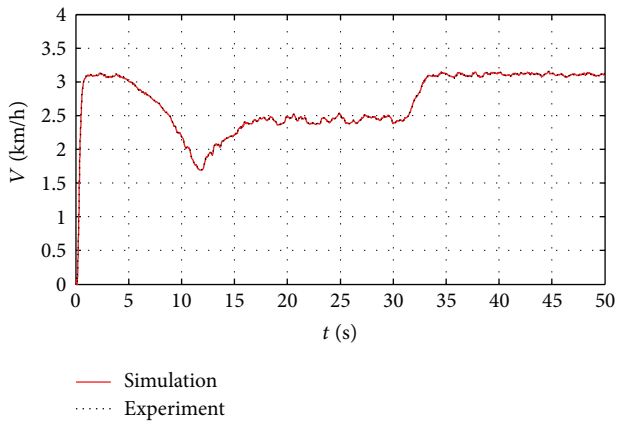

Figure 7: Bulldozer velocities in the simulation and experiment.

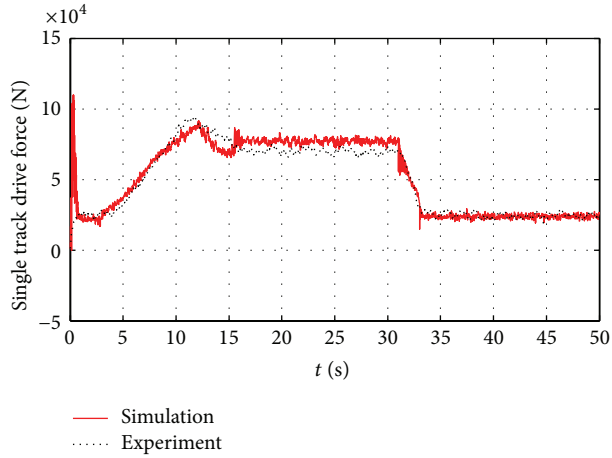

Figure 8: Single track drive forces in the simulation and experiment.

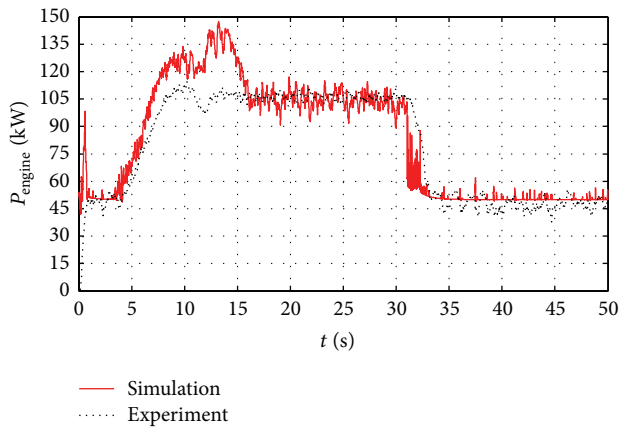

Figure 9: Engine output power in the simulation and experiment.

under the working condition shown in Figure 6. Figure 9 shows the engine output power in the simulation and experiment. Figure 10 shows the generator and motor efficiency under the working condition.

As we can see from Figures 7 to 8, bulldozer velocities and single track drive forces in the simulation and experimental data are identical well. As can be seen from data, the variance's relative error of the single track drive forces in the simulation and experimental data is 1.45%.

In Figure 9, the engine output power in the simulation and experimental data are identical well-expected 4–16 s soil-cutting stage. The engine output power in simulation is higher about 15~25 kW than that in experiment in 4–16 s soil-cutting stage. This is because the efficiency of the power train system is different in simulation (hybrid) and experiment (traditional).The experiment transmission efficiency is set approximately 0.9, which is higher than that of simulation transmission. Figure 10 shows that the simulation efficiency is below 0.90 for motor in 4–16 s soil-cutting stage. So the engine must provide higher power in simulation than that in experiment in order to satisfy the same demand power of the bulldozer.

Under the state above, the simulation model (Figure 5) is valid and can be used for the simulation research of control strategy for the hybrid electric tracked bulldozer.

4. Control Strategy

4.1. Power Allocation Strategy. One power follow control strategy is put forward to combine the working features of the proposed series hybrid electric tracked bulldozers, which should be able to coordinate the power supply and need relationship among the engine generator, ultracapacitor, and the motors. The engine output power should follow the load demand power of the bulldozer, and the ultracapacitor should supply the power shortage caused by the excessive load demand power as the auxiliary power source. The SOC of the ultracapacitor and load power requirement determines the working point of the engine generator. The power allocation strategy is shown in Table 2.

In Table 2, P^* is the target demand mechanical power; P_e is engine output power; P_{e_max} is engine maximum output power; P_{e_min} is engine minimum output power; P_{DC} is DC

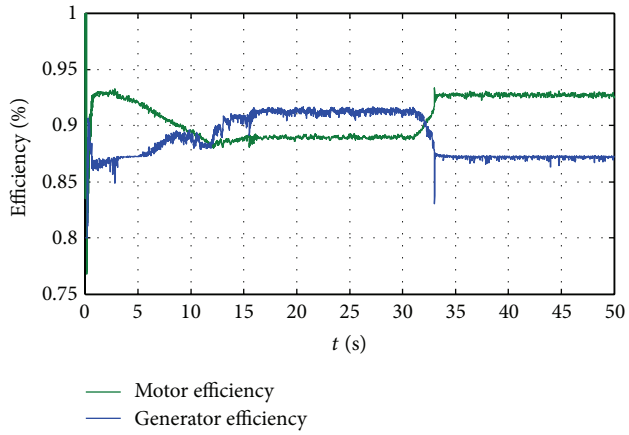

Figure 10: Generator and motor efficiency.

Table 2: Power allocation strategy.

Judgment	State of the ultracapacitor	Power supply
$P^* < P_{e\_max}$ $SOC < SOC_{max}$	Charging	$P_g = \eta_1 * P_e$ $P_{uc} = P_{DC} - P_g$
$P^* < P_{e\_max}$ $SOC \geq SOC_{max}$	Not working	$P_g = \eta_1 * P_e$ $P_{uc} = 0$
$P^* > P_{e\_max}$ $SOC > SOC_{min}$	Discharging	$P_g = \eta_1 * P_{e\_max}$ $P_{uc} = P_{DC} - P_g$
$P^* > P_{e\_max}$ $SOC \leq SOC_{min}$	Not working	$P_g = \eta_1 * P_{e\_max}$ $P_{uc} = 0$

BUS demand electric power; P_g is generator output power; P_{uc} is ultracapacitor power; η_1 is power efficiency of the generator; SOC_{max} and SOC_{min} are ultracapacitor maximum and minimum state of charge, respectively.

P^* is target demand mechanical power, which can be given as

$$P^* = \frac{P^*_{Track}}{\eta_{E\text{-}T}} = \frac{F_{Track} * r}{\eta_{E\text{-}T}} = \frac{(F_E + F_T) * r}{\eta_{E\text{-}T}}, \quad (15)$$

where P^*_{Track} is the demand power of the track; $\eta_{T\text{-}E}$ is the transmission efficiency from engine to track; F_{Track} is the off-road motion resistance; F_E is external travel resistance calculated by (1)~(2); F_T is operating resistance calculated by (3).

As can be seen from (15) and (1)~(3), we can conclude that the average cutting depth h_p and the volume of the mound in front of the bulldozing plate V are linear to P^*; P^* is a quadratic function of the track amount of sinkage Z. These primary parameters h_p, V, and Z impact the energy management at the above level.

The flowchart for the power allocation strategy is shown in Figure 11. The driver's intention is taken as the target required power P^*, and the vehicle management system (VMS) calculates the drive motor required power P^*_m according to the working conditions of all components and the vehicle. Simultaneously, the VMS calculates the engine target speed n^* and the ultracapacitor target current I^*. The engine-generator set makes the output power P_{eg}, whereas the ultracapacitor makes the output power P_{uc} according to a data table lookup. The output power of the engine-generator set and ultracapacitor is then sent to the drive motors through DC BUS.

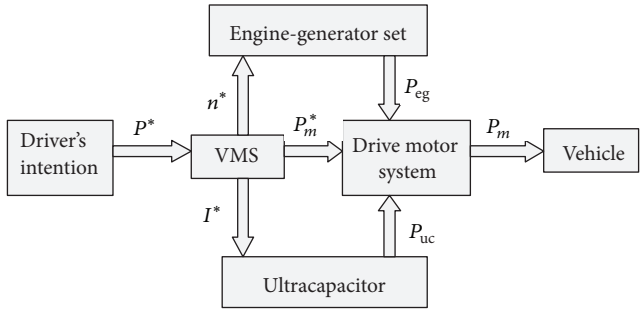

Figure 11: The flowchart for the power allocation strategy.

Table 3: Parameters of the control strategy.

Parameters	Instructions
SOC_{max}	Maximum SOC
SOC_{min}	Minimum SOC
N_1	Engine working speed 1
N_2	Engine working speed 2
N_3	Engine working speed 3

In this control strategy, the parameters must be properly adjusted and optimized to reduce fuel consumption as much as possible in order to satisfy the operational requirements. The parameters of the control strategy are shown in Table 3.

4.2. Engine Control Strategy. An engine multipoint speed switching control strategy is adopted here, and engine working speed is determined by the bulldozer load demand power. The engine operates at low speeds when the load demand power is low and operates at higher speeds when the load demand power increases. Figure 12 shows the schematic of the engine multipoint speed switching control strategy.

In Figure 12, x-axis represents engine speed and y-axis represents load demand power. Load demand power is divided into three areas: low, medium, and high. The engine speed in each area is fixed as N_1, N_2, and N_3. When the load demand power is in low load area, engine speed will be fixed at N_1; as load demand power increases to medium load area, engine speed will be fixed at N_2; as load demand power increases to high load area, engine speed will be fixed at N_3. Power hysteresis band is set between each adjacent load power area to avoid the engine speed frequent switching.

4.3. Real Experimental Testing of Control Strategy. Test bench experiment was performed to collect actual test bench data to correlate and validate the proposed power follow control strategy for this hybrid electric tracked bulldozer. The experimental bench consists of engine, generator, drive

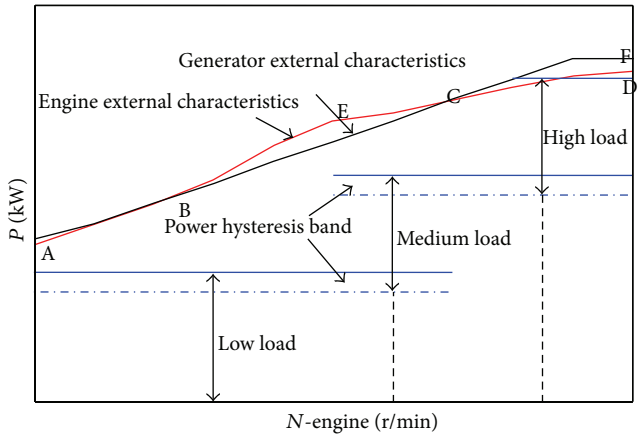

FIGURE 12: Schematic of the engine multipoint speed switching control strategy.

TABLE 4: Basic parameters of the power train system.

Name	Value	Unit
Maximum power of the engine (P_{e_max})	175	kW
Rated power of the motor (P_{m_rated})	75	kW
Maximum power of the motor (P_{m_max})	105	kW
Rated power of the generator (P_{g_rated})	175	kW
Maximum power of the generator (P_{g_max})	180	kW

motor system, auxiliary power source, dynamometer, and the vehicle management system, as shown in Figure 13(a).

This test bench adopts power follow control strategy which was written in the vehicle management system to coordinate the power supply among the engine generator and the motors. Dynamometer control interface shown in Figure 13(b) controls the working speed of the dynamometer and drive motor, and the drive motor controller controls the load torque of the drive motor. In the process of test, the load torque of the drive motor was increased up from 30 N·m to 100 N·m suddenly and then down to 30 N·m suddenly to simulate the load sudden changes process of the bulldozer, as shown in Figure 14. Load torque is linear related to the accelerator pedal opening degree.

As we can see from the test bench result shown in Figure 15, the engine-generator output power follows the load demand power well under the working condition shown in Figure 14. Under the state above, the proposed power follow control strategy is effective and can be used for the control strategy optimization for the hybrid electric tracked bulldozer.

5. Control Strategy Optimization

5.1. Optimization Model. To solve the problem of the parameter optimization of the power follow control strategy, a mathematical model of the entire power train system including the fuel consumption model is established based on the dynamic modeling in Section 3 and the control strategy in Section 4. The important parameters of the power train system of the bulldozer are given in Table 4.

The fuel consumption model is obtained through the fuel consumption MAP graph shown in Figure 16, where b_e (g/Kwh) is fuel consumption rate. Minimizing fuel consumption is the optimization goal, and the working condition has no effect on the control strategy put forward here. Therefore, one representative bulldozer working condition is adopted here, as shown in Figure 17.

In this optimization problem, the object function is engine fuel consumption under the representative working condition. Engine minimum fuel consumption can be obtained by integration [27]:

$$\min B = \int_{t_0}^{t_1} B\left(n, P_e, t\right) dt, \tag{16}$$

where B is engine fuel consumption; n is engine speed at time t; P_e is engine output power at time t; and t_0 and t_1 are the start and end time of the bulldozer working condition, respectively.

In this problem, the SOC of the ultracapacitor at the start and end times should remain identical. Therefore, the sum of the ultracapacitor output and input energies is zero:

$$\int_{t_0}^{t_1} P_{\mathrm{uc}}\left(t\right) dt = 0,$$
$$\mathrm{SOC}_{\min} \le \mathrm{SOC} \le \mathrm{SOC}_{\max}. \tag{17}$$

The other constraint conditions are the following:

$$P_{e\_\min} \le P_e \le P_{e\_\max},$$
$$n_{e\_\min} \le n_e \le n_{e\_\max}, \tag{18}$$
$$I_{\mathrm{uc}} \le I_{\mathrm{uc\_max}},$$

where $n_{e\_\max}$ and $n_{e\_\min}$ are the maximum and minimum speeds of the engine, respectively, and $I_{\mathrm{uc\_max}}$ is the maximum charging/discharging current of the ultracapacitor.

5.2. Control Strategy Optimization. Based on the characteristics of the series hybrid tracked bulldozer, a genetic algorithm (GA) is adopted to solve the parameter optimization problem in the control strategy. The engine working speeds N_1, N_2, and N_3 at different power levels are set as the objective optimized parameters. The initial values of N_1, N_2, and N_3 are determined by engineering experience. Because GA cannot address the parameters directly, the parameters must be converted into a chromosome composed of genes with a certain structure. Therefore, the chromosome here is X_i (N_1, N_2, N_3). The GA operations are as follows: selection, crossover, and mutation.

A design of experiment (DOE) is used to simplify the calculation. As a design space exploration technique, DOE is used for preliminary design space exploration to reflect the relationship between the design variables and objective function in fewer numbers of trials. According to the given optimization variables, 16 test sample points are constructed

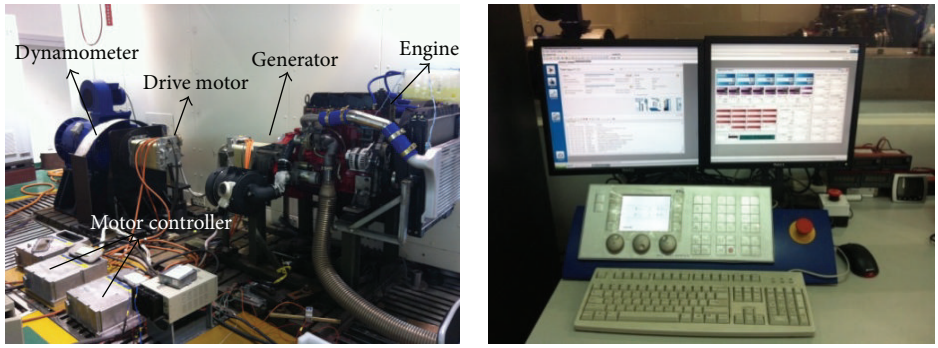

(a) (b)

Figure 13: Hardware setup for experiments. (a) Structure of the hybrid bulldozer test bench; (b) dynamometer control interface.

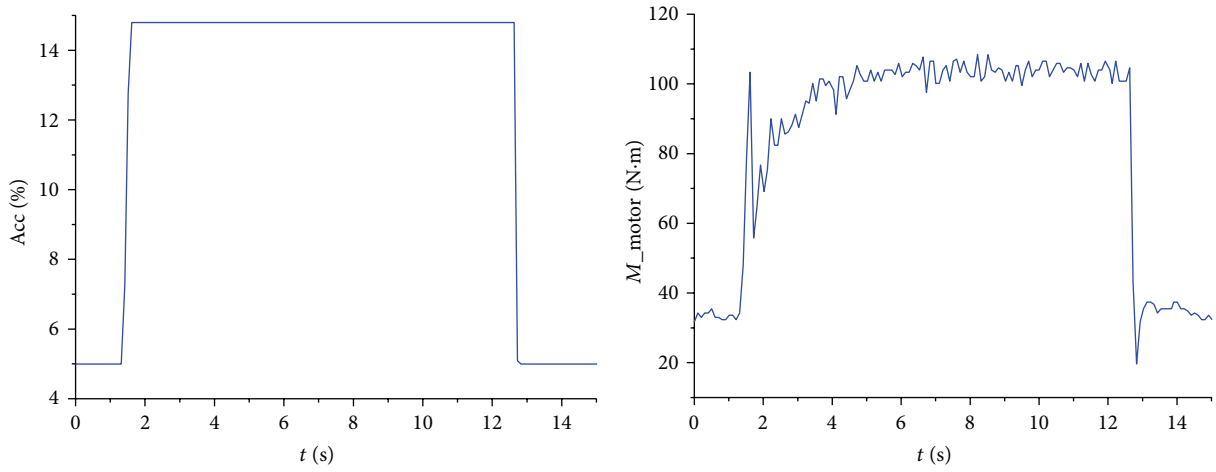

(a) Accelerator pedal opening degree (b) Load torque of the drive motor

Figure 14: The test bench working condition.

using an orthogonal design method. The response surface is constructed on the basis of the DOE and can replace the original model with certain accuracy. On the basis of the DOE, the GA is then applied to optimize the parameters in the solution space to determine the optimal solution [28, 29]. The GA work flow is then established (Figure 18) by setting the minimum fuel consumption as the target function under typical working conditions.

In this flowchart, $f(x)$ and $g_j(x)$ are the objective function and constraint conditions given in (16)~(18). The main optimization steps are as follows: (1) initialize the first-generation chromosomes randomly, X_i, $i = 1$; (2) simulate the control strategy parameters represented by each chromosome using the vehicle simulation model for one complete simulation and determine the fitness of each individual according to the predetermined fitness function; (3) select a new generation of chromosomes, X_i', according to the fitness values (the selected probability is greater when the fitness is larger); (4) crossover and mutate, to generate the new chromosomes, X_i, $i = i + 1$; (5) return to (2); and (6) halt the process when satisfying the stopping condition.

Table 5: Optimization results for the parameters.

Parameters	Before optimization	After optimization
N_1 (rpm)	1000	1102
N_2 (rpm)	1400	1395
N_3 (rpm)	1650	1621
B (g)	4200	3917

5.3. Optimization Results. Figure 19 shows the convergence process of the control strategy parameters and the objective function under the combined simulation. N_1, N_2, and N_3 are the engine working speeds at the engine power ranges of 0–60 kW, 60–120 kW, and 120–175 kW, respectively. With the proceeding of the optimization process, N_1, N_2, and N_3 are constantly adjusted in the engine working speed range and gradually converge to stable values.

After 16 optimization calculations, through the optimization in software environment of OPTIMUS, one solution in the solution space is finally found as the optimal (Table 5).

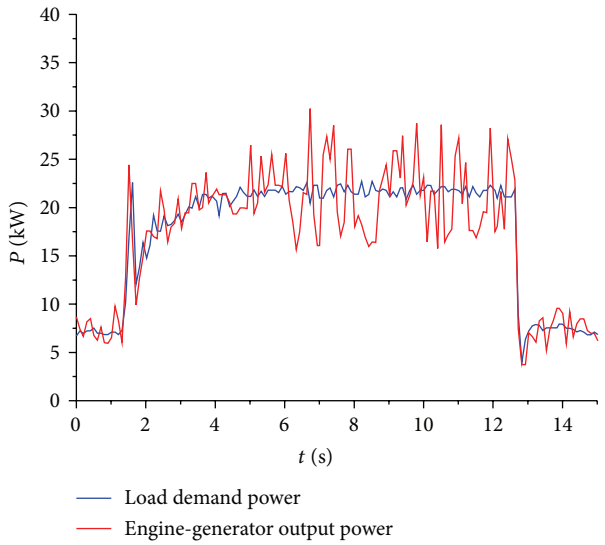

Figure 15: Engine-generator output power and load demand power.

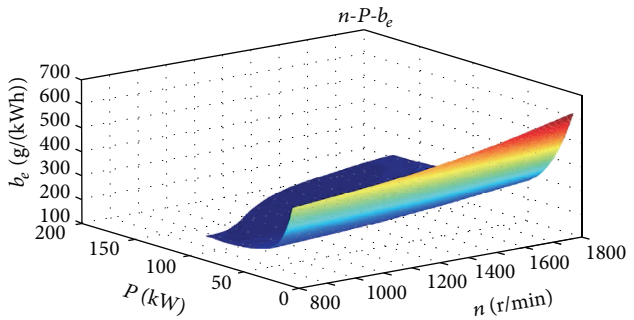

Figure 16: Fuel consumption MAP graph.

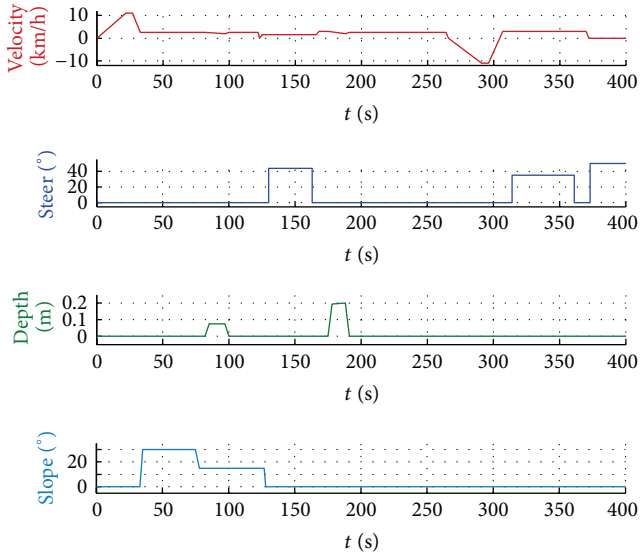

Figure 17: Typical working conditions of the bulldozer.

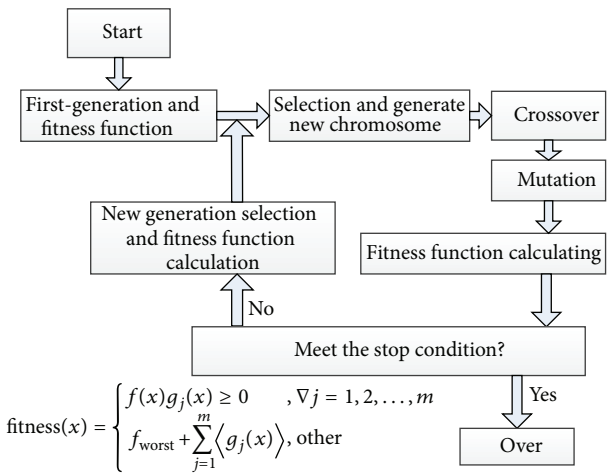

Figure 18: The GA flowchart of the control strategy optimization.

Figure 20 shows the right and left track velocity of the hybrid bulldozer under the typical working condition (Figure 17). As shown in Figure 21, the adjustment of the engine speed is great after optimization, especially in low load power and high load power areas. Engine speed was adjusted from low efficiency to high efficiency working point to improve the fuel economy of the bulldozer as shown in Figure 22.

The adjustment of the engine speed impacts the power allocation in a certain degree. As can be seen from Figure 21, in the high load power area, the engine maximum output power decreased due to the decreasing of the engine speed after adjustment. Under the same working condition, the ultracapacitor power supplement will be increased when the demand power is very large. Discharge current will increase to reduce the life of the ultracapacitor to some extent.

6. Conclusions

Based on the study of the terramechanics of the tracked bulldozer and test bench experimental data, a dynamic model of the hybrid electric tracked bulldozer power train system was established, combining the operation principle of each part of the system. To verify the accuracy of the dynamic simulation model, the parameters and the real working conditions of the prototype traditional bulldozer were substituted into the simulation model, and the simulation results were compared with the experimental data to analyze the accuracy of the simulation model. A power follow strategy is proposed, combining the working features of the series hybrid electric tracked bulldozer. Test bench experiment was performed to collect actual test bench data to correlate and validate the proposed power follow control strategy for this hybrid electric tracked bulldozer. Based on the dynamic model of this hybrid electric tracked bulldozer, a genetic algorithm is proposed to solve the control strategy parameter optimization problem. Based on the optimized control strategy parameters, the simulation is performed to compare engine fuel consumption before and after control strategy optimization. By analyzing the optimization results, the fuel consumption of the bulldozer after optimization is reduced by approximately 6.74% compared

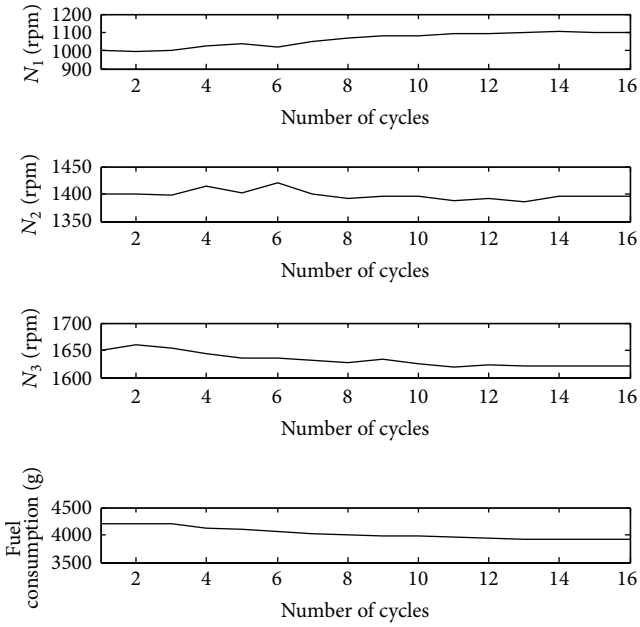

Figure 19: The convergence process of the objective function.

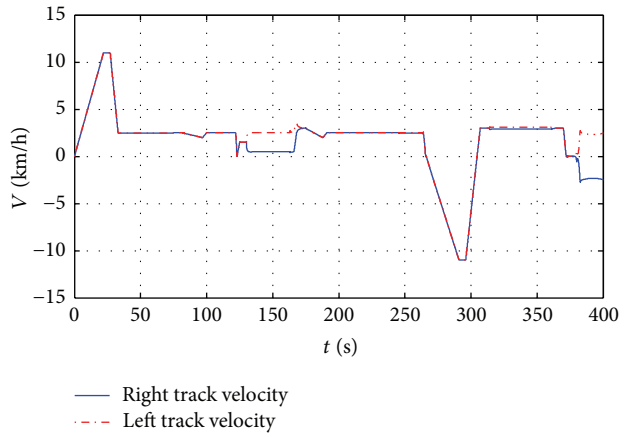

Figure 20: The right and left track velocities of the bulldozer.

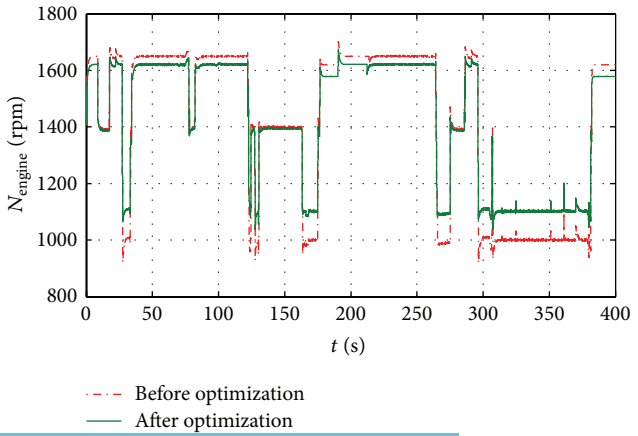

Figure 21: Comparison of engine speed.

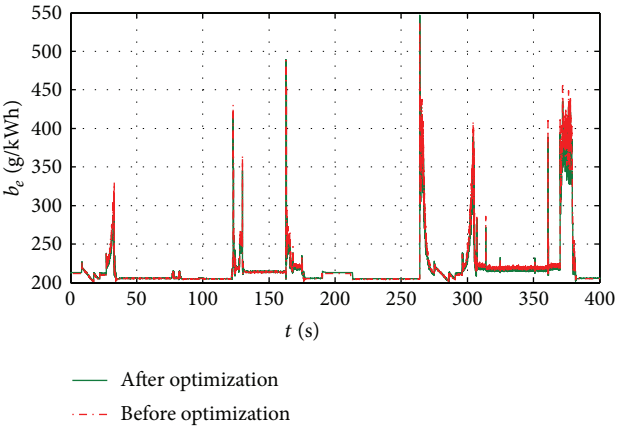

Figure 22: Comparison of engine fuel consumption.

with the former condition. This result verifies the validity of the method proposed in this paper which can reduce the difficulty of the design and optimize the control strategy.

Conflict of Interests

The authors declare no conflict of interests regarding the publication of this paper.

Acknowledgment

The authors gratefully acknowledge the support from the National Key Technologies R&D Program of China (Grant no. 2011BAG04B02).

References

[1] H. Wang and F. C. Sun, "Dynamic modeling and simulation on a hybrid power system for dualmotor—drive electric tracked bulldozer," *Applied Mechanics and Materials*, vol. 494-495, pp. 229–233, 2014.

[2] Q. Song and H. Wang, "Parameters matching for dual-motor-drive electric bulldozer," *Journal of Beijing Institute of Technology*, vol. 20, pp. 169–170, 2011.

[3] J. Wang, Q. N. Wang, P. Y. Wang, J. N. Wang, and N. W. Zou, "Hybrid electric vehicle modeling accuracy verification and global optimal control algorithm research," *International Journal of Automotive Technology*, vol. 16, no. 3, pp. 513–524, 2015.

[4] C. Sun, X. Hu, S. J. Moura, and F. Sun, "Velocity predictors for predictive energy management in hybrid electric vehicles," *IEEE Transactions on Control Systems Technology*, vol. 23, no. 3, pp. 1197–1204, 2015.

[5] R. Ghorbani, E. Bibeau, P. Zanetel, and A. Karlis, "Modeling and simulation of a series parallel hybrid electric vehicle using REVS," in *Proceedings of the American Control Conference (ACC '07)*, pp. 4413–4418, IEEE, New York, NY, USA, July 2007.

[6] P. Caratozzolo and M. Canseco, "Design and control of the propulsion system of a series hybrid electric vehicle," in *Proceedings of the Electronics, Robotics and Automotive Mechanics Conference (CERMA '06)*, pp. 270–273, Mexico, Russia, September 2006.

[7] Z. Y. Song, H. Hofmann, J. Q. Li, J. Hou, X. B. Han, and M. G. Ouyang, "Energy management strategies comparison for

electric vehicles with hybrid energy storage system," *Applied Energy*, vol. 134, pp. 321–331, 2014.

[8] X. Hu, L. Johannesson, N. Murgovski, and B. Egardt, "Longevity-conscious dimensioning and power management of the hybrid energy storage system in a fuel cell hybrid electric bus," *Applied Energy*, vol. 137, pp. 913–924, 2015.

[9] X. Y. Li, X. M. Yu, J. Li, and Z. X. Wu, "Control strategy for series hybrid-power vehicle," *Journal of Jilin University (Engineering and Technology Edition)*, vol. 2, pp. 122–126, 2005.

[10] E. Mehrdad, Y. Gao, and A. Emadi, *Modem Electric, Hybrid Electric, and Fuel Cell Vehicles: Fundamentals, Theory, and Design*, CRC Press, New York, NY, USA, 2010.

[11] X. Hu, N. Murgovski, L. Johannesson, and B. Egardt, "Energy efficiency analysis of a series plug-in hybrid electric bus with different energy management strategies and battery sizes," *Applied Energy*, vol. 111, pp. 1001–1009, 2013.

[12] C. Sun, S. J. Moura, X. Hu, J. K. Hedrick, and F. Sun, "Dynamic traffic feedback data enabled energy management in plug-in hybrid electric vehicles," *IEEE Transactions on Control Systems Technology*, vol. 23, no. 3, pp. 1075–1086, 2015.

[13] R. Xiong, H. He, Y. Wang, and X. Zhang, "Study on ultracapacitor-battery hybrid power system for PHEV applications," *High Technology Letters*, vol. 16, no. 1, pp. 496–500, 2010.

[14] T.-S. Kwon, S.-W. Lee, S.-K. Sul et al., "Power control algorithm for hybrid excavator with supercapacitor," *IEEE Transactions on Industry Applications*, vol. 46, no. 4, pp. 1447–1455, 2010.

[15] G. G. Wang, I. Horowitz, S. H. Wang, and C. W. Chen, "Control design for a tracked vehicle with implicit nonlinearities using quantitative feedback theory," in *Proceedings of the 27th IEEE Conference on Decision and Control*, pp. 2416–2418, IEEE, Austin, Tex, USA, December 1988.

[16] Y. H. Li, X. M. Lu, and N. C. Kar, "Rule-based control strategy with novel parameters optimization using NSGA-II for power-split PHEV operation cost minimization," *IEEE Transactions on Vehicular Technology*, vol. 63, no. 7, pp. 3051–3061, 2014.

[17] S. Zhang, C. N. Zhang, R. Xiong, and W. Zhou, "Study on the optimal charging strategy for lithium-ion batteries used in electric vehicles," *Energies*, vol. 7, no. 10, pp. 6783–6797, 2014.

[18] J. K. Peng, H. W. He, and N. L. Feng, "Simulation research on an electric vehicle chassis system based on a collaborative control system," *Energies*, vol. 6, no. 1, pp. 312–328, 2014.

[19] C. M. Qi and P. Li, "An exponential entropy-based hybrid ant colony algorithm for vehicle routing optimization," *Applied Mathematics & Information Sciences*, vol. 8, no. 6, pp. 3167–3173, 2014.

[20] K. B. Wipke, M. R. Cuddy, and S. D. Burch, "ADVISOR 2.1: a user-friendly advanced powertrain simulation using a combined backward/forward approach," *IEEE Transactions on Vehicular Technology*, vol. 48, no. 6, pp. 1751–1761, 1999.

[21] L. Guzzella and A. Amstutz, "CAE tools for quasi-static modeling and optimization of hybrid powertrains," *IEEE Transactions on Vehicular Technology*, vol. 48, no. 6, pp. 1762–1769, 1999.

[22] J. H. Pu, C. L. Yin, and J. W. Zhang, "Application of genetic algorithm in optimization of control strategy for hybrid electric vehicles," *China Mechanical Engineering*, vol. 16, Article ID 649650, 2005.

[23] M. G. Bekker, *Off-Road Locomotion*, The University of Michigan Press, Ann Arbor, Mich, USA, 1960.

[24] C. G. Zhang, K. H. Zeng, and J. H. Zhao, "Analytical solutions of critical load and Terzaghi's ultimate bearing capacity for unsaturated soil," *Journal of Tongji University (Natural Science)*, vol. 38, no. 12, pp. 1736–1739, 2010.

[25] G. Bekker M, *Theory of Land Locomotion*, The University of Michigan Press, Ann Arbor, Mich, USA, 1956.

[26] Q. Song, P. Zeng, and H. Wang, "Study on the power flowing control strategy of a series hybrid tracked bulldozer at the typical working condition," *Journal of Mechanical Engineering*, vol. 50, no. 2014, pp. 136–143, 2014.

[27] R. C. Wang, R. He, J. B. Yu, and C. H. Hu, "Parameter optimization of a PSHEV based on genetic algorithm," *China Mechanical Engineering*, vol. 24, no. 18, pp. 2544–2549, 2013.

[28] A. Piccolo, L. Ippolito, V. Zo Galdi, and A. Vaccaro, "Optimisation of energy flow management in hybrid electric vehicles via genetic algorithms," in *Proceedings of the IEEE/ASME International Conference on Advanced Intelligent Mechatronics*, pp. 434–439, Como, Italy, July 2001.

[29] B. Wang, Z. P. Yang, F. Lin, and W. Zhao, "An improved genetic algorithm for optimal stationary energy storage system locating and sizing," *Energies*, vol. 7, no. 10, pp. 6434–6458, 2014.